Molecular Vision 2026; 32:265-279 <http://www.molvis.org/molvis/v32/265>
Received 6 May 2025 | Accepted 2 July 2026 | Published 5 July 2026

SS31 protects damaged retinal cells through the AMPK/DRP1 signaling pathway

Na Cui,[1,2] Rui-xue Zhang,[1,2] Qian Yang,[3] Yuan Ren,[1,2] Jun Jia,[1,2] Xia Wang,[1,2] Xu Liu,[1,2] Yuan He[1,2]

[1]Department of Ophthalmology, The Second Affiliated Hospital of Xi'an Medical University, Xi'an, Shaanxi, P.R. China; [2]Xi'an Key Laboratory for the Prevention and Treatment of Eye and Brain Neurological Related Diseases, Xi'an, Shaanxi, P.R. China; [3]Department of Chinese Materia Medica and Natural Medicines, School of Pharmacy, Air Force Medical University, Xi'an, Shaanxi, P.R. China; The first two authors contributed equally to this study.

Purpose: Glaucoma is a group of neurodegenerative diseases characterized by progressive loss of retinal ganglion cells (RGCs) and optic nerve fibers. Mitochondrial dynamics contribute to the maintenance of neuronal homeostasis, and abnormalities can lead to the development of glaucoma. SS31 is a mitochondria-targeting short peptide that has been found to protect mitochondrial function and thereby protect damaged retina-associated cells. The aim of this study is to investigate whether SS31 protects damaged retinal cells by activating the AMPK/DRP1 pathway.
Methods: The relationship between SS31 and oxidative stress was determined by live-cell imaging. The cells were inoculated in the well plate and treated with H_2O_2 (150 μM) for 24 h and pretreated with or without SS31 (100 nM), AICAR (17.5 μM), or dorsomorphin (7 μM) for 2 h. 3-(4,5-dimethylthiazol-2-yl)-2,5-diphenyltetrazolium bromide (MTT) and lactate dehydrogenase (LDH) were used to evaluate cell viability. Mitochondrial genetic stability was detected by droplet digital PCR. The expression of AMPK and DRP1 was detected by western blot. In addition, intraocular pressure and retinal thickness were evaluated in mice with acute ocular hypertension.
Results: SS31 inhibited H_2O_2-induced cell death of 661W through the AMPK signaling pathway and maintained mitochondrial genetic stability. SS31 regulates AMPK/Drp1 signaling in 661W cells after oxidative stress. SS31 reduced intraocular pressure and maintained normal retinal thickness in mice with acute ocular hypertension.
Conclusions: SS31 regulates mitochondrial dynamic network remodeling by activating AMPK/DRP1 signaling pathway and protects retinal-related cells.

Glaucoma, a group of diseases characterized by progressive optic nerve degeneration, is a leading cause of irreversible blindness worldwide. Glaucoma, which is classified into various subtypes depending on the structural changes in the anterior segment of the eye, is expected to affect more than 100 million people worldwide by 2040 [1]. The characteristic pathological change in glaucoma is the death of retinal ganglion cells (RGCs), which ultimately causes visual field loss and irreversible blindness [2]. Intraocular pressure (IOP) is the only treatable risk factor [3]; however, not all patients with glaucoma have elevated IOP, and not all patients with elevated IOP develop glaucoma. Lowering IOP is not sufficient to prevent disease progression. The focus of glaucoma pathogenesis is to understand the structural and functional impairment of the mitochondria and their axons and synapses in RGCs [4]. Elevated IOP, aging, genetic variation, immune dysfunction [5], oxidative stress [6], and neurotrophin deficiency [7] are potential triggers of mitochondrial dysfunction in glaucoma [8]. Therefore, understanding the potential mechanisms and relationships between mitochondrial structural and functional alterations will facilitate the development of mitochondria-associated neuroprotection against glaucomatous neurodegeneration in RGCs, their axons, and synapses.

Mitochondrial dysfunction is caused by abnormal mitochondrial dynamics [9]. Excessive mitochondrial division is associated with mitochondrial breakage, whereas excessive mitochondrial fusion leads to mitochondrial lengthening [10]. Dynamin-related protein 1 (Drp1) is a genetically encoded GTPase [11], which, when activated, is recruited to the outer mitochondrial membrane, where it oligomerizes in a GTP-dependent manner and restricts mitochondrial function, leading to mitochondrial breakage [12]. AMP-activated protein kinase (AMPK), a cellular energy sensor, plays a key role in regulating mitochondrial homeostasis [13]. In studies on cardiovascular calcification, melatonin activates AMPK expression, decreases Drp1 expression, and subsequently inhibits mitochondrial fission, which in turn reduces apoptosis and calcium deposition [14]. In heat stress–induced hepatic injury, shengmusan promotes the phosphorylation of AMPK, which maintains mitochondrial homeostasis through Drp1-dependent mitochondrial phagocytosis processes [15].

Correspondence to: Yuan He, Department of Ophthalmology, The Second Affiliated Hospital of Xi'an Medical University, No. 167, Fangdong Street, Xi'an, Shaanxi, 710038, P.R. China; email: heyuan@xiyi.edu.cn

These studies suggest that AMPK is a molecular bridge between energy metabolism and mitochondrial function, with the AMPK/Drp1 pathway regulating mitochondrial division [16,17].

As a novel water-soluble mitochondria-targeted short peptide, SS31 can freely cross the cell membrane and selectively concentrate on the inner mitochondrial membrane; its concentration in mitochondria can reach 1,000 to 5,000 times that in the cytoplasm without saturation [18-21]. Furthermore, SS31 targets mitochondria for the treatment of cardiovascular [22] and renal diseases [23]. SS31 has potential applications in neurodegenerative pathologies such as Alzheimer's disease [24], Parkinson's disease [25], and Huntington's chorea [26], where the mitochondrial structure is abnormal and dysfunctional. In recent years, researchers have proposed that SS31, a novel neuroprotective agent, has a protective effect against glaucoma [27,28]. SS31 protects human lens epithelial cells cultured in vitro by reducing the mitochondrial damage caused by oxidative injury [29]. Our previous study showed that SS31 protects the mouse retinal photoreceptor cell line 661W through mitochondrial autophagy [30], but its molecular mechanism of action remains unclear. Therefore, this study aimed to investigate the mechanism by which SS31 restores the neuroprotective role of retina-associated cells by regulating mitochondrial dynamic network remodeling through activation of the AMPK/Drp1 pathway, which provides an experimental basis for SS31 in the clinical treatment of glaucoma.

METHODS

Cell culture and animals: The murine retinal photoreceptor cell line 661W was obtained from the American Type Culture Collection (Manassas, VA) and maintained in Dulbecco's modified Eagle's medium (Thermo Fisher Scientific, Waltham, MA) supplemented with 10% fetal bovine serum (Thermo Fisher Scientific). The cells were treated in the following experiments with 75% to 80% confluence. All data were generated from the average of three independent experiments performed on each sample, each assay in triplicate. All 661W cells used in this experiment were within five passages. Before conducting the experiment, we performed short tandem repeat (STR) authentication on the 661W cells (Appendix 1), and the results showed that both negative and positive detection results were correct. Amplification map of Genomic DNA clear and genotyping results were good. The STR analysis results showed that no more than two distinct alleles were found at only two loci, suggesting the sample derived from a common ancestry (Appendix 2). There are no matched cell lines in these databases of ExPASy (Appendix 3).

The mice were treated in accordance with the ARVO Statement for the Use of Animals in Ophthalmic and Vision Research, and experiments were approved by the Xi'an Medical University Animal Ethics Committee (Approval No. XYLS2019134). Eight-week-old male mice were provided by the Laboratory Animal Center of Xi'an Medical University, China, and housed normally before the experiment.

Cell viability: The viability of 661W cells under H_2O_2 toxicity was estimated using MTT and LDH release assays. Cells were seeded into the 96-well plates and treated with H_2O_2 (150 μM), with or without pretreatment of SS31 (100 nM, 2 h), AICAR (17.5 μM, 2 h), or dorsomorphin (7 μM, 2 h), respectively, for 24 h. After treatment, cells were incubated with 10 μl MTT (Thermo Fisher Scientific) for 4 h. Then, the medium was removed, and 150 μl dimethyl sulfoxide was added to each well, which was then shaken for 10 min. Absorbance at 490 nm was measured using a microplate reader. For the LDH assay, 661W cells in 96-well plates were cultured with 100 μL of the LDH reaction mixture in the dark for 30 min. Then, the reaction was terminated, and a microplate reader was used to read the absorbance at 490 nm.

Cell growth curve measurement: The 661W-mKate2 cell was labeled by the mKate2-encoding lentivirus from CytoBiotech (Hangzhou, China), and successfully transfected cells exhibited red fluorescence in the nucleus under fluorescence microscopy. The positive rate after antibiotic screening was more than 99%. The 661W cells were inoculated into 96-well plates with 100 μl per well, with five replicates per experimental group and a positive control. After administration (1 μM SS31, 150 μM H_2O_2), the 96-well cell culture plate was placed in a 37 °C incubator for 10 min and then put into an incubator equipped with a live-cell imaging system, IncuCyte ZOOM (Essen Bioscience, Ann Arbor, MI), to incubate and perform real-time dynamic live-cell imaging to monitor changes in cell proliferation. The parameters of the real-time dynamic live-cell imaging system were set to automatically capture bright-field and red fluorescence images, and dynamic images at 1 h/time and 4 fields/holes/time. In the living cell state, the nucleus steadily emits bright red fluorescence. Through IncuCyte ZOOM automatic software and database analysis, changes in cell proliferation, hypertrophy, and other phenomena are monitored and visually reflected by cell confluence values and curves.

Droplet digital PCR test: The microdroplet was prepared and transferred to a 96-well PCR reaction plate (approximately 45–55 μl). The 96-well plate was covered with heat-sealing film. After sealing the film, PCR amplification should be

Name	Primer (5'-3')	Number of bases	5 'modifier	3 'modifier
ND1-F1	CTCAACCTAGCAGAAACAAACC	22		
ND1-F2	CTCAACCCTAGCAGAAACAAACC	23		
ND1-R	GGCCGGCTGCGTATTCTAC	19		
ND1-P	CCCCCTTCGACCTGACAGAAGGAGA	25	5′-VIC	3′-BHQ1

performed within 30 min or within 4 h at 4 °C in a refrigerator. A 96-well plate was sealed and cycled in an ETC 811 gene amplification apparatus (Bio-Rad, Hercules, CA) under the following cycling protocol: 95 °C for 10 min (DNA polymerase activation), followed by 45 cycles of 95 °C for 30 s (denaturation) and 60 °C for 1 min (annealing), followed by an infinite 16 °C hold. The reaction plate was amplified and detected with a MicroDROP-100B biochip reader (Guangzhou Forevergen Biosciences, Guangshou, China). The droplet detector was preheated for 30 min, and the data results were analyzed using Quant-Drop data analysis software (Seoul, South Korea). The sequence of primers used is shown in Table 1.

Western blot analysis: After treatment, 661W cells in a six-well plate were harvested using RIPA buffer and centrifuged. The supernatant was used for protein quantification and denaturation using a BCA protein assay kit (Pierce Chemical, Rockford, IL). Equal amounts of protein were separated using sodium dodecyl sulfate–polyacrylamide gel electrophoresis and transferred to polyvinylidene fluoride membranes (Millipore, Bedford, MA). The western blotting analysis was performed using antibodies against AMPK (ab133448; Abcam, Cambridge, MA) and DRP1 (ab193216; Abcam). The immune complexes were visualized using an Immobilon Western Chemiluminescent HRP substrate (WBKLS; MILLIPORE, San Diego, CA) according to the manufacturer's instructions.

Establishment of a mouse model of acute high intraocular pressure glaucoma and measurement of intraocular pressure: A mouse model of acute ocular hypertension glaucoma was established with or without pretreatment of SS31 (100 μM, 200 μM, 2 h), AICAR (17.5 μM, 2 h), or dorsomorphin (7 μM, 2 h). Male C57BL/6J mice (6–8 weeks old) were obtained from the Laboratory Animal Center of Xi'an Medical University (Xi'an, China). The animals were housed in standard cages under specific pathogen-free conditions, with free access to food and water, and maintained on a 12-h light/dark cycle. A retinal ischemia-reperfusion (RIR) animal model was established by inducing acute intraocular hypertension, as previously described [31]. Briefly, mice were anesthetized via intraperitoneal injection of pentobarbital sodium (100 mg/kg), and 0.5% procaine (Alcon, Fort Worth, TX, USA) was topically applied to the left eye. The pupil was dilated by applying 1% tropicamide (Santen, Osaka, Japan) to the cornea. The anterior chamber was cannulated with a 33-gauge needle connected to a normal saline reservoir, which was then elevated to 150 cm and maintained in this position for 90 min. This procedure resulted in a sustained average intraocular pressure (IOP) of 110 mm Hg. For the control group, sham surgery was performed without IOP elevation. Following the procedure, the needle was removed to allow IOP to return to normal levels. Levofloxacin eye drops (Santen) were administered to prevent infection. Eyes exhibiting cannulation-induced cataract, iris injury/bleeding, or anterior chamber leakage were excluded from the study. IOP was measured in both eyes using a TonoLab rebound tonometer (Colonial Medical Supply, Franconia, NH, USA) after the mice were anaesthetized. IOP was measured before perfusion; 15 min, 30 min, and 1 h during perfusion; and 1 h, 6 h, 24 h, 3 days, and 7 days after perfusion. Six correct single measurements were used for each eye to generate an average IOP reading.

Intravitreal injection of SS31: On the ultra-clean table, SS31 was first prepared into a 5-μl sterile solution, and a leak-proof device with a 33-gauge needle with a ground tip and a 10-μl microinjector was assembled and calibrated. After anesthesia with 1.5% isoflurane in mice, 1% topiramate was dropped to dilate the pupils. The eyelid area was gently wiped clean with 75% ethanol and fixed with a 37 °C heating pad. Under a microscope, the eyeball was exposed, and a needle was inserted 1 mm into the vitreous cavity at a 30° angle, 1.5 mm behind the corneal edge and above the temporal region. SS31 was injected at a rate of 1 μl/s, and then the needle point was gently pressed for 2 s after removal to prevent vitreous leakage. Antibiotic eye ointment was dropped. Finally, the mice were transferred to a 37 °C environment for resuscitation, and the eyes were observed 3 to 7 days after surgery to be alert for complications such as endophthalmitis and retinal detachment.

Histopathology: After the mice were sacrificed under deep anesthesia, their eyes were dissected at the designated time points, fixed with FAS eye fixative (HaoKe Bio, Hangzhou,

China), and then subjected to paraffin embedding after gradient dehydration with gradually increasing ethanol. Prepare slices (5 μm thick) spanning the optic nerve of each eye and stain them with hematoxylin and eosin (HE). For each retina, four 200 × 200-μm^2 observation areas were selected at a distance of 1 mm from the optic disc, and the measurements were repeated by two blind researchers. The microstructure changes of the mouse retina were collected and analyzed using a Nikon Eclipse optical microscope (Nikon, Tokyo, Japan), and the inner plexiform layer (IPL) thickness and cell count of the retinal ganglion cell layer were quantitatively determined by ImageJ (National Institutes of Health, Bethesda, MD) software. The retinal ganglion cell layer is a key functional layer in the retina's multilayered structure, located in the innermost layer (near the vitreous body). It is the "last stop" and "output port" for visual signals to be transmitted from the retina to the brain. Its core function is to convert the light signals processed by the cells in the anterior layer of the retina into neural electrical signals and form the optic nerve through axons to transmit them to the visual center of the brain.

Statistical analysis: All data are reported as mean ± standard deviation. One-way analysis of variance, followed by a Bonferroni post hoc test, was used to compare differences among more than two groups, and a two-tailed unpaired Student's *t* test was used to assess differences between two groups using GraphPad Prism version 9.0 software (GraphPad Software, La Jolla, CA). *P* values less than 0.05 indicated statistical significance.

Ethics approval and consent to participate: Ethical approval was granted by the Research Ethics Committee of Xi'an Medical University, Shaanxi, China. All animal experiments and procedures were approved by the Ethics Committee for the Use of Laboratory Animals of Xi'an Medical University, China. The ethical approval number is XYLS2020110.

RESULTS

Real-time dynamic live-cell imaging system to monitor 661W cell growth: To study the relationship between SS31-mediated neuroprotection and oxidative stress, we first monitored the changes in proliferation and hypertrophy of 661W cells using the real-time dynamic live-cell imaging system, and the results were reflected by the phase object fusion and curves. 661W-mKate2 cells could grow and proliferate normally in a serum-free medium, but the cellular growth cycle or doubling time was prolonged. H_2O_2 can damage the 661W-mKate2 cells and inhibit their growth and proliferation. Treatment of 661W-mKate2 cells with 1 μM SS31 for 4 h and 10 h had no significant effect on cell proliferation. Exposure of 661W-mKate2 cells to H_2O_2 for 4 h or 10 h damaged the cells and inhibited their growth and proliferation. The growth and proliferation of damaged cells were restored after treatment with 1 μM SS31 for 10 h. There were no significant changes in the growth and proliferation of damaged cells after treatment with 1 μM SS31 for 4 h and 6 h (Figure 1).

SS31 attenuated H_2O_2-induced 661W cell death via the AMPK signaling pathway: SS31 significantly reduced H_2O_2-induced 661W cell death. Moreover, the AMPK activator AICAR enhanced the protective effect of SS31, whereas the AMPK inhibitor dorsomorphin reduced its protective effect. The results of phase-contrast microscopy showed that H_2O_2 exacerbated 661W cell death, while SS31 inhibited the effect of H_2O_2. The protective effect of SS31 was enhanced in the presence of AICAR; however, the protective effect of SS31 was diminished in the presence of dorsomorphin (Figure 2A). The MTT and LDH assays confirmed these results (Figure 2B, C).

SS31 maintained mitochondrial genetic stability through the AMPK signaling pathway: The results of droplet digital PCR experiments showed that the mitochondrial DNA (mtDNA) copy number of H_2O_2-damaged cells was significantly lower than that of the control group, whereas the copy number of oxidatively damaged cells pretreated with SS31 was significantly higher than that of the H_2O_2-damaged group. The copy number in 661W cells treated with AICAR was significantly higher than that in the control and SS31 groups. In addition, dorsomorphin treatment significantly decreased the mtDNA copy number. SS31 and AICAR/dorsomorphin pretreatment resulted in a significant decrease in the copy number of oxidized cells compared with the SS31 pretreatment injury group (Figure 3).

Effect of SS31 on the AMPK/Drp1 signaling pathway: Immunoprotein blotting showed no significant change in AMPK and Drp1 expression in the SS31-treated group; AMPK and Drp1 expression were increased in the AMPK activator AICAR-treated group, whereas AMPK and Drp1 expression were decreased in the AMPK inhibitor dorsomorphin-treated group. Application of H_2O_2 significantly decreased the expression of AMPK and Drp1, while the addition of SS31 treatment on the basis of injury significantly increased the expression of AMPK and Drp1. Concomitant addition of AICAR resulted in an even more significant increase in the expression of AMPK and Drp1, whereas SS31 treatment with the concomitant addition of dorsomorphin resulted in a significant decrease in the expression of AMPK, and Drp1 expression did not change significantly (Figure 4A–C). These results suggest that SS31 modulates AMPK/Drp1 signaling after oxidative stress.

Alteration of IOP in an acute high-IOP glaucoma mouse model: A mouse model of acute high-IOP glaucoma was established using a hypertonic saline injection in the anterior chamber (Figure 5A). There was no significant difference in

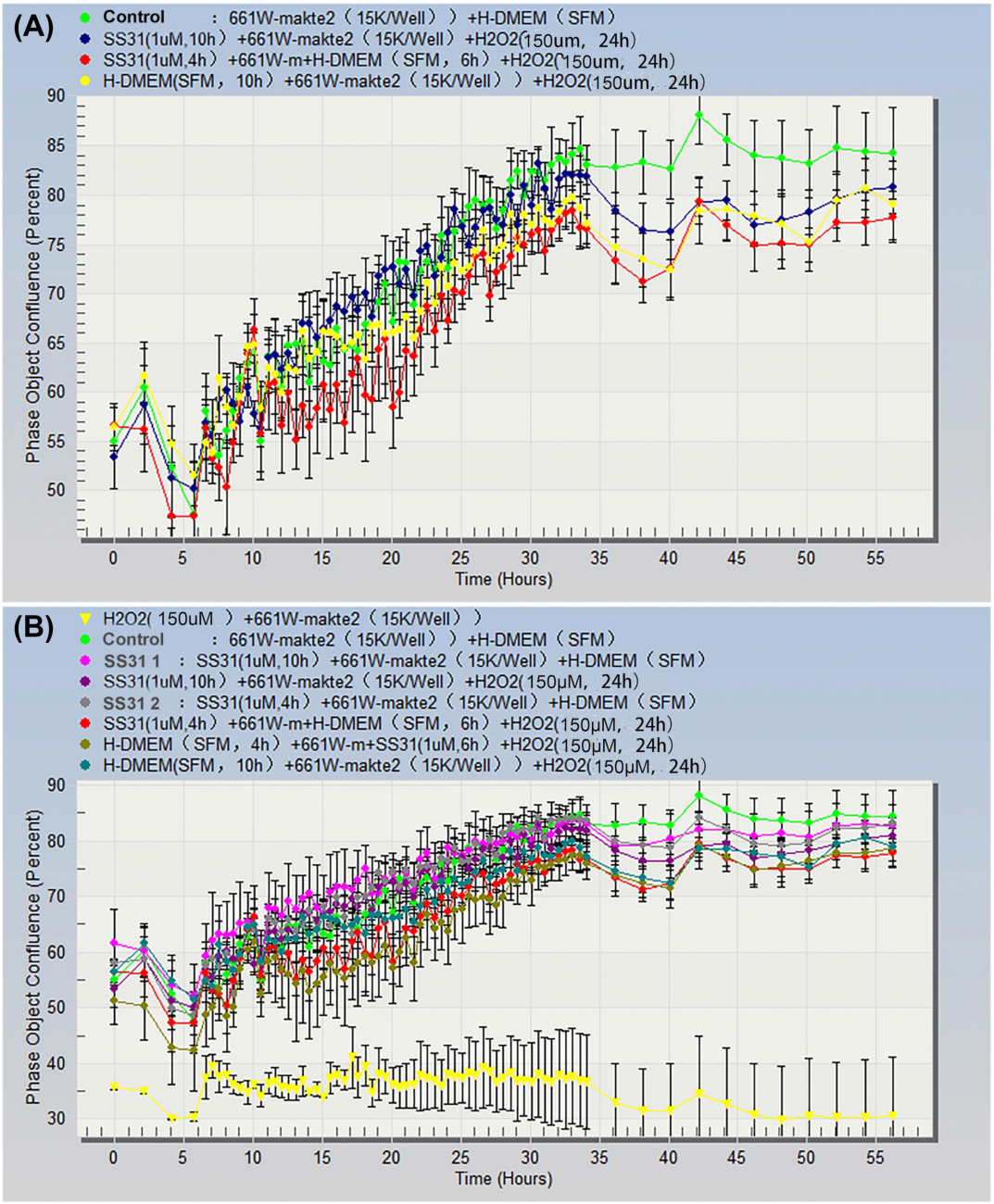

Figure 1. Real-time dynamic live-cell imaging cell confluence and growth curves of 661W cells. 661W-makte2 cells were passaged for model injury and drug administration according to the experimental protocol, placed in a 37 °C incubator for 10 min, and then put into a real-time dynamic live-cell imaging system to monitor the changes in cell proliferation (n = 6). Real-time dynamic live-cell imaging was used to record the growth and proliferation curves of 661W cells in the normal group, H_2O_2 treatment group, and SS31 treatment group. **A**. The green curve represents the normal control group, the yellow curve represents the oxidative damage group, the dark blue curve represents the SS31 monotherapy group, and the red curve represents the SS31 combined with H_2O_2 treatment group. **B**. The green curve represents the normal control group, the yellow and cyan curves represent the oxidative damage group, the rose red and gray curves represent the SS31 monotherapy group, and the purple, red, and yellow-green curves represent the SS31 combined with the H_2O_2 treatment group.

IOP among the four groups before perfusion. As shown in Figure 5B, a rapid and significant increase in the IOP was observed immediately after perfusion. The IOP peaked at 1 h of perfusion and slowly decreased after perfusion was stopped. The IOP in the SS31 (100 μM), SS31 (200 μM), and AICAR (17.5 μM) groups showed the same trend. At 15 and 30 min of perfusion, the IOP in the perfusion-only group was significantly different from that in the SS31 (100 μM), SS31 (200 μM), and AICAR (17.5 μM) groups. On days 1 and 3 after the cessation of perfusion, there was a significant difference in the IOP of the perfusion-only group compared with the SS31 (100 μM) and AICAR (17.5 μM) groups.

Intravitreous injection of SS31 can alleviate postperfusion retinal injury: According to histopathological analysis, compared with the control group, the number of RGCs in acute glaucoma mice pretreated with or without SS31 was significantly reduced, and the number of RGCs was not increased after extended testing days, indicating that RGC damage caused by high-pressure saline perfusion is irreversible. In mice with acute glaucoma the reduction in the number of RGCs was significantly higher in the group with intravitreous SS31 injection than in the group without SS31 pretreatment (Figure 6A, B).

Intravitreal injection of dorsomorphin aggravated retinal damage: Compared with the control group, the number of RGCs and retinal thickness in the dorsomorphin treatment group decreased significantly, and the number of RGCs and retinal thickness decreased gradually with the increase of time. Compared with 1 day of dorsomorphin treatment, the number of RGCs and retinal thickness decreased more significantly after 3 days of dorsomorphin treatment (Figure 7A, B).

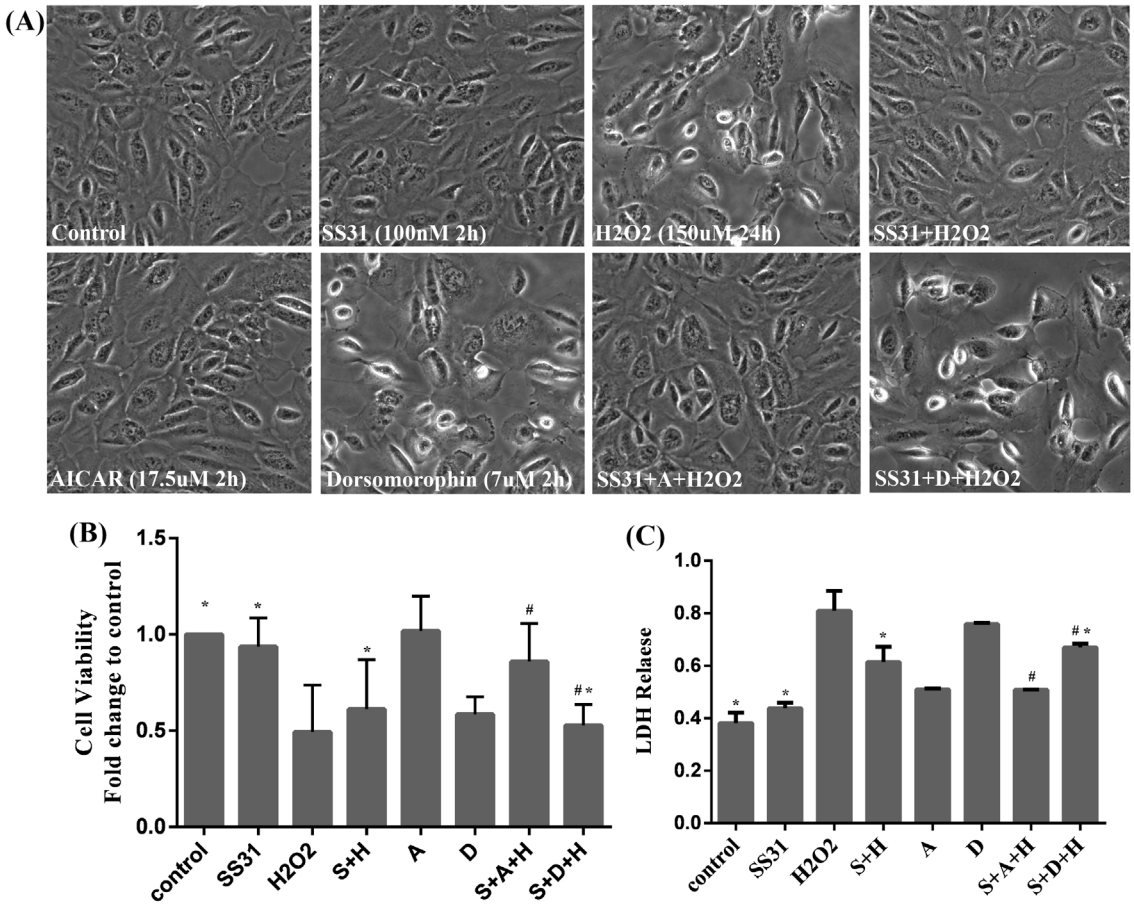

Figure 2. Effect of SS31 on H_2O_2-induced 661W cell death via the AMPK signaling pathway. **A**. Morphological map of 661W cells under a phase-contrast microscope shown. Scale bar: 50 μm. **B**. Cell viability assay by the MTT assay. *Significantly different from H_2O_2, $p < 0.05$. #Significantly different from S+H, $p < 0.01$. n = 35. **C**. LDH assay. *Significantly different from H_2O_2, $p < 0.05$. #Significantly different from S+H, $p < 0.01$. n = 6. A, AICAR; D, dorsomorphin; H, H_2O_2.

Intravitreous injection of SS31 and AICAR alleviated post-perfusion retinal injury: Compared with the control group, the number of RGCs in mice with acute glaucoma pretreated with or without SS31 and AICAR decreased significantly, but the retinal thickness did not change significantly. Compared with the perfusion group, the number of RGCs in the SS31 and AICAR pretreatment groups was significantly increased, but the retinal thickness was not significantly changed. After 1 day of perfusion, the number of RGCs in the SS31 and AICAR pretreatment groups did not decrease, indicating that SS31 and AICAR had a protective effect on RGCs (Figure 8A, B).

DISCUSSION

The pathogenesis of glaucoma is complex, and the underlying mechanisms and factors are unclear. The recognized risk factors include pathological intraocular pressure, glutamate excitotoxicity, immune abnormalities, and mitochondrial abnormalities [1]. Mitochondrial targeted peptide SS31 is a novel ophthalmic drug that has neuroprotective effects on glaucoma models [27,28] and can also reduce oxidative stress–induced cell damage [29,30]. Treatment with 1 μM SS31 for 10 h can restore the growth and proliferation of 661W cells damaged by H_2O_2. Retinal mitochondrial dynamics are disrupted in patients with glaucoma, and Drp1 inhibitors can protect retinal cells [4]. The AMPK/Drp1 pathway is crucial for related treatments [15,31], and AMPK can downregulate Drp1 [32,33]. Alzheimer's disease, which has a similar mechanism to glaucoma, can be treated with Drp1 inhibitors combined with SS31 [34]. Regulating mitochondrial fission to maintain homeostasis is crucial for reducing related diseases.

A total of 150 μmol/l H_2O_2 was used to stimulate 661W cells for 24 h to establish a model of oxidative damage in the pathogenesis of glaucoma. Based on the previous experimental study [35], 100 nmol/l SS31 was chosen for the treatment of 661W cells. The AMPK activator AICAR and the inhibitor dorsomorphin were used as positive controls. These results revealed that SS31 significantly reduced H_2O_2-induced 661W cell death. Moreover, the AMPK activator AICAR enhanced the protective effect of SS31, whereas the AMPK inhibitor dorsomorphin reduced its protective effect. Corresponding results were obtained for the mitochondrial genetic stability assay, in which SS31 and AICAR increased the copy number of mtDNA, whereas dorsomorphin decreased the copy number. Translational validation of the oxidative damage model based on transcriptomic observations revealed that the addition of SS31 treatment on top of the damage resulted in a significant increase in the expression of AMPK and Drp1, which was even more pronounced when AICAR was added, while the addition of dorsomorphin to the SS31 treatment resulted in a significant decrease in the expression of AMPK and no significant increase in the expression of

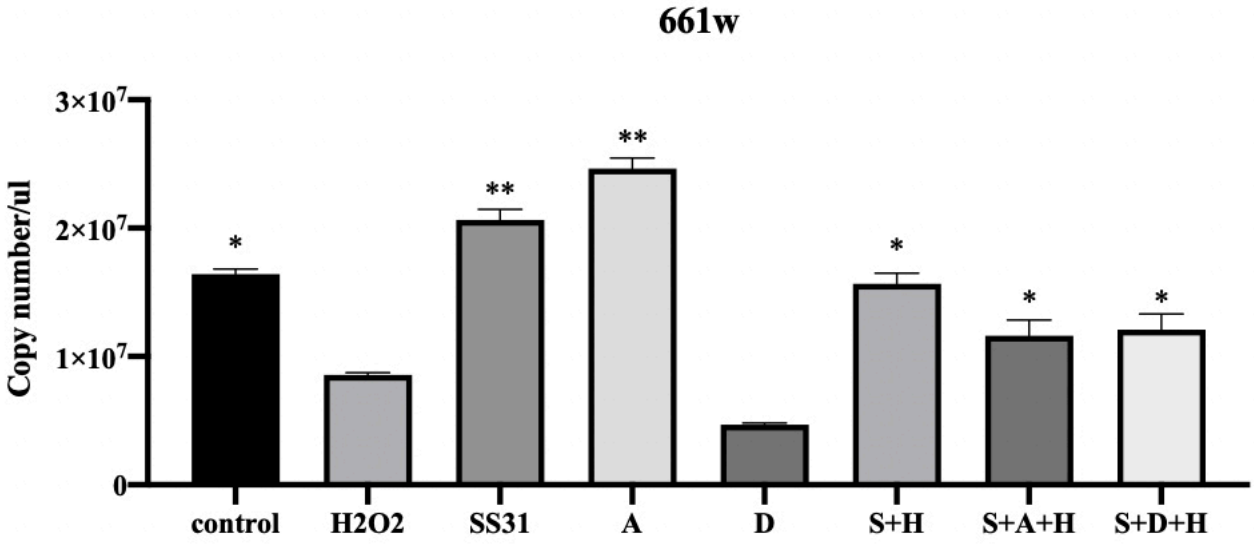

Figure 3. Effect of SS31 on mitochondrial genetic stability through the AMPK signaling pathway. The mitochondrial DNA (mtDNA) in each group of 661W cells was quantified by droplet digital PCR, and the absolute copy number of the mtDNA was analyzed by Quant-Drop quantification software to identify positive and negative droplets. *Significantly different from H_2O_2, $p < 0.05$. **Significantly different from H_2O_2, $p < 0.01$. n = 6.

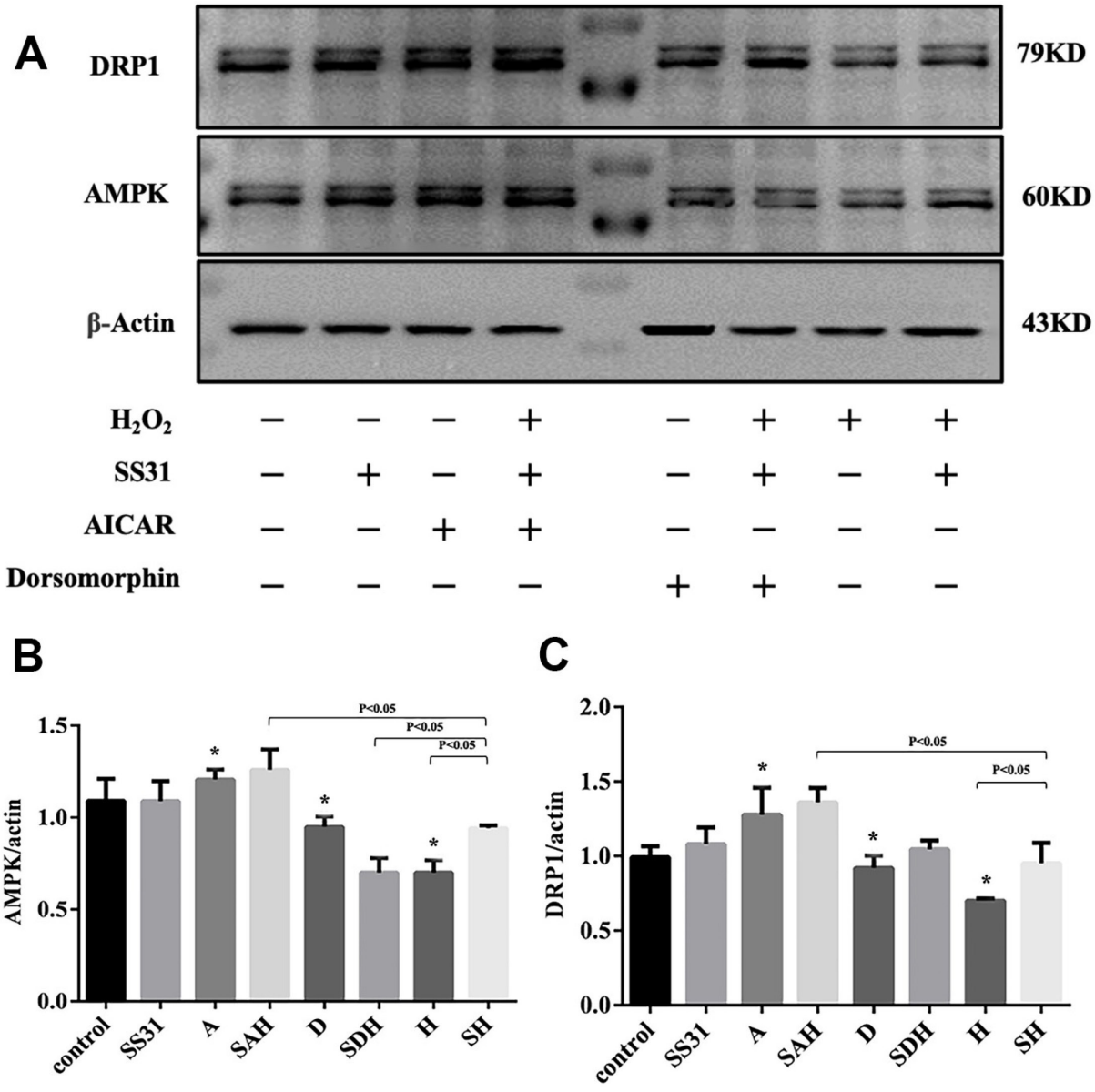

Figure 4. Effect of SS31 on AMPK and Drp1 expression in 661W cells. **A–C**: Western blot (**A**) and density analysis (**B**, **C**) of 661W cell lysates treated with 24-h hydrogen peroxide (150 μM), SS31 (100 nM, 2 h) with or without pretreatment, AICAR (17.5 μM, 2 h), or dorsomorphin (7 μM, 2 h). Application of H_2O_2 significantly decreased the expression of AMPK and Drp1, while the addition of SS31 treatment on the basis of injury significantly increased the expression of AMPK and Drp1. *Significantly different from H_2O_2, $p < 0.05$. n = 6.

Drp1. However, Drp1 expression did not change significantly. Interestingly, SS31 treatment had no effect on the expression of AMPK and Drp1 in a normal cell model, echoing phase-contrast microscopy and transcriptome experiments.

IOP is a dynamic parameter that reflects fluctuations in IOP over a 24-h period and provides a reference for the treatment of glaucoma. It has been found that optic nerve damage in experimental glaucoma animal models is closely associated with abnormally elevated IOP and the duration of high pressure [36]. Induction models leading to high IOP include laser-induced high IOP [37], anterior chamber injection of hypertonic saline [38], cauterization of the external scleral vein [39], and injection of hyaluronic acid, microspheres, and magnetic or nonmagnetic microbeads [40-43]. In this study, a mouse model of acute high-IOP glaucoma was established by injecting hypertonic saline

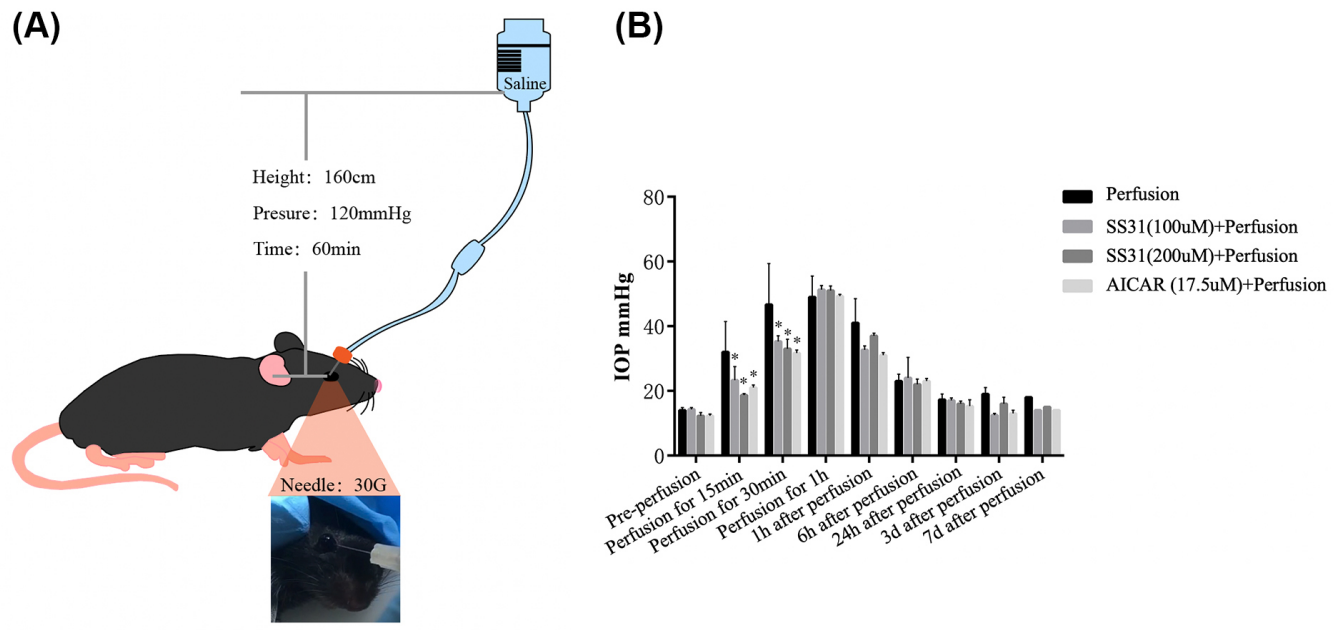

Figure 5. Measurement of intraocular (IOP) pressure in a mouse model of acute high-IOP glaucoma. **A**. Construction of a mouse model of acute high-IOP glaucoma presented. **B**. Measurement of intraocular pressure in mice after perfusion in each group. IOP values are expressed as the mean ± standard deviation of each time point. After 15 min of perfusion, the IOP of the mice increased significantly at each time point. In the perfused 15-min, 30-min, 1-h, 3-day, and 7-day groups, the IOP of mice pretreated with different concentrations of SS31 and AICAR was lower than that of the perfused group. Data are from three independent experiments. *Significantly different from the preperfusion group, $p < 0.05$. n = 6.

into the anterior chamber. Glaucoma is the leading cause of irreversible blindness worldwide and encompasses a group of diseases characterized by optic nerve atrophy and visual field defects [44]. Acute glaucoma, one of the most common types of glaucoma in Asia, is characterized by a sudden and dramatic increase in IOP, leading to RIR injury and RGC death [45]. Acute IOP elevation is a key driver of retinal inflammation and optic nerve damage, often accompanied by microglial activation and dysregulated ferroptosis pathways [46]. Therefore, we employed the mouse RIR model induced by hypertonic normal saline and an in vitro oxidative stress model to investigate the pathogenesis of acute glaucoma. Among these models, the RIR model is an internationally recognized animal model for exploring the pathogenesis of acute glaucoma [47]. Immediately after perfusion, a rapid and significant increase in IOP was observed, with IOP reaching a peak at 1 h of perfusion and then slowly decreasing after cessation of perfusion; the difference in IOP between the perfusion-only group and the different experimental groups was obvious. According to histopathological analysis, the number of RGCs was significantly reduced in the intravitreous SS31 injection group compared with the group without SS31 pretreatment. Compared with the control group, the number of RGCs and retinal thickness in the dorsomorphin treatment group decreased significantly, and the number of RGCs and retinal thickness decreased gradually with the increase in time. Compared with the control group, the number of RGCs in mice with acute glaucoma pretreated with or without SS31 and AICAR decreased significantly, but the retinal thickness did not change significantly. The changes in IOP before and after infusion have been repeatedly verified and found to be associated with the protective effect of SS31, although its effect is short-lived. For the damage of the ganglion cell layer caused by acute ocular hypertension, SS31 preconditioning has been proven to have an obvious protective effect on the ganglion cell layer.

Although we have explored both in vitro and in vivo the protective effects of SS31 on damaged retina-associated cells and its regulatory role in mitochondrial dynamics via activation of the AMPK/DRP1 pathway, this conclusion is derived from specific experimental settings: the 661W cell model and acute injury models. Its efficacy in chronic glaucoma models or across other retinal cell types remains to be clarified. Given the variability in cell types and microenvironments, the specific biologic effects of SS31 may differ under distinct

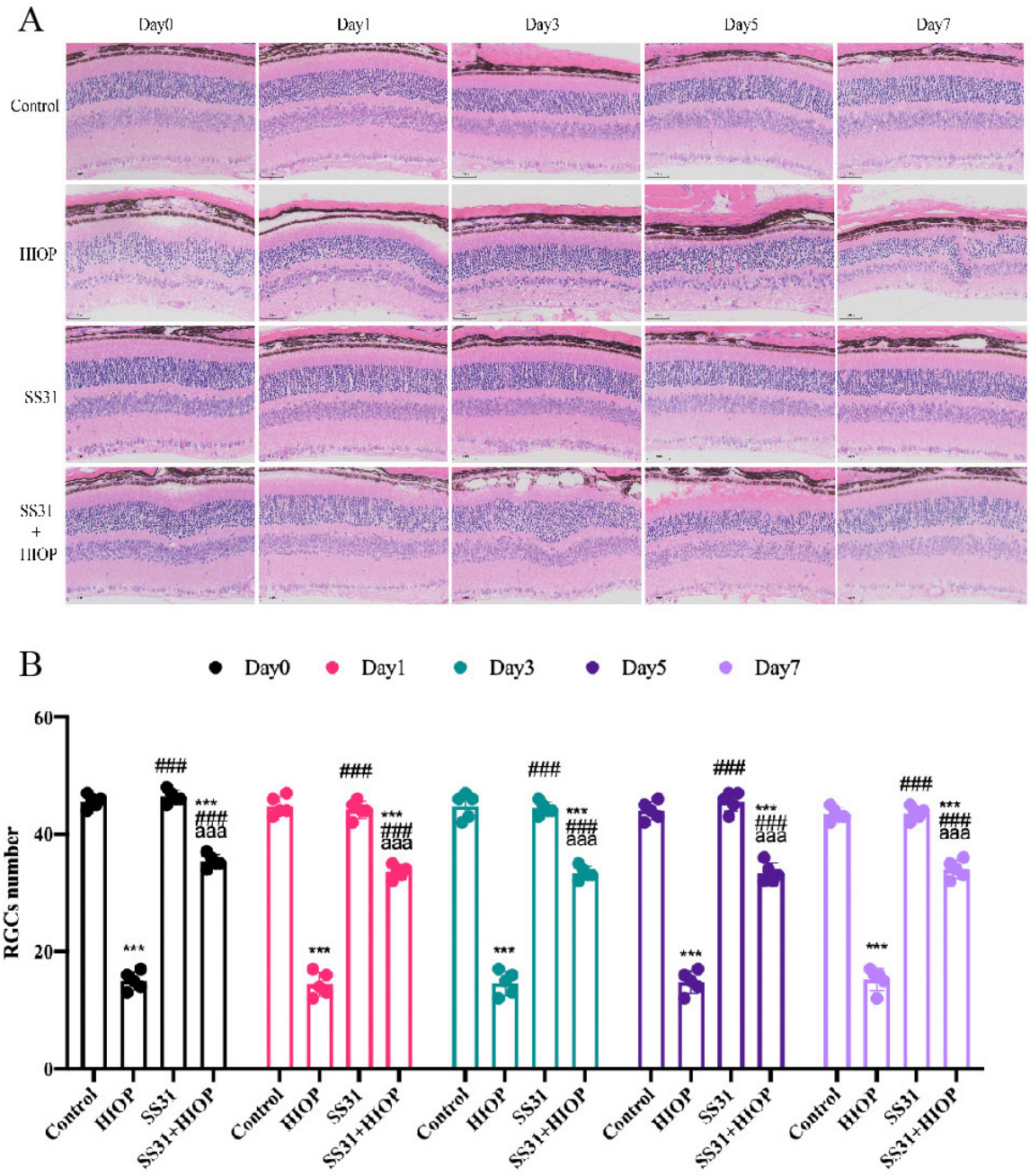

Figure 6. Intravitreous injection of SS31 can alleviate postperfusion retinal injury. **A**, **B**: Statistical analysis of hematoxylin and eosin staining and retinal ganglion cell quantity in the retina of mice at 0, 1, 3, 5, and 7 days after SS31 pretreatment or no SS31 pretreatment shown. *Significantly different from control. ***$p < 0.001$. #Significantly different from chronic high intraocular pressure (HIOP). ###$p < 0.001$, significantly different from SS31. $^{aaa}p < 0.001$. n = 6. Scale bar: 50 µm.

conditions, necessitating further investigations to validate these findings.

Conclusions: In this study, we reported the protective effects of the novel targeted peptide SS31 on 661W cells and on the retinas of mice with acute high-IOP glaucoma under oxidative stress conditions. We found that SS31 protects oxidatively damaged retina-associated cells by regulating mitochondrial dynamic network remodeling through activation of the AMPK/Drp1 pathway, which in turn plays an important role in the optic nerve treatment of glaucoma.

APPENDIX 1. THE METHOD OF 661W CELL STR CERTIFICATION.

To access the data, click or select the words "Appendix 1." 1) The centrifuge tube symbolizes sample processing, representing the processes of cell lysis and DNA extraction. 2) The reagent kit and PCR machine symbolize reagent preparation and amplification reaction, enabling simultaneous amplification of multiple targets. 3) The ABI 3730XL instrument (a classic capillary electrophoresis platform) and computer represent the separation and signal acquisition processes. 4) The peak graph symbolizes the allelic detection results of STR loci, visually displaying the "genetic fingerprint" of cells. 5) The computer + magnifying glass symbolize "search and comparison," verifying through the database whether the cells are the target strain or contaminated.

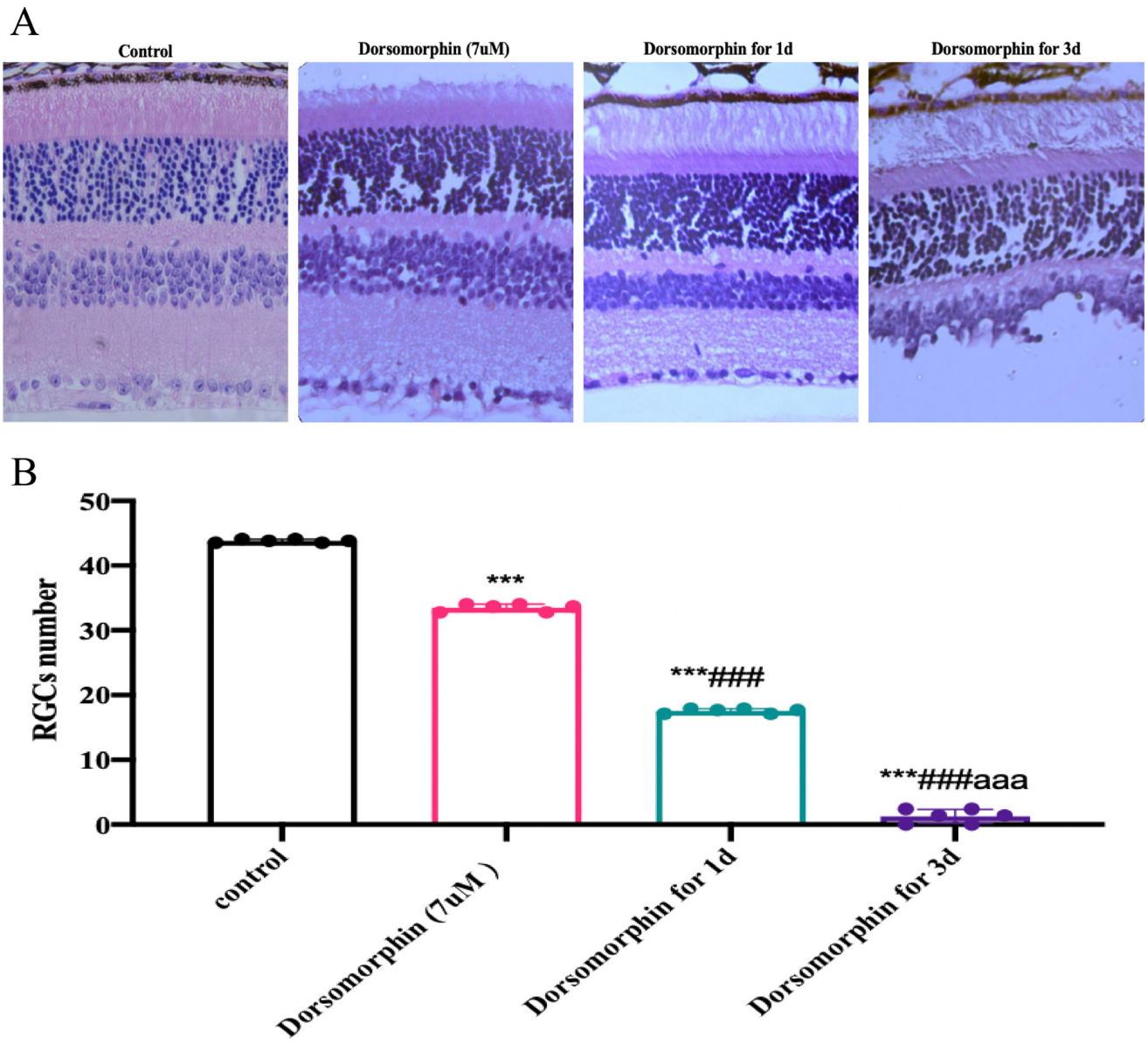

Figure 7. Intravitreal injection of dorsomorphin aggravated retinal damage. **A**, **B**: Statistical analysis of retinal hematoxylin and eosin staining and retinal ganglion cell quantity in mice treated with dorsomorphin (7 µM, 2 h) for 1 and 3 days shown. These retinas have not received treatment for high intraocular pressure. *Significantly different from control. ***$p < 0.001$. #Significantly different from dorsomorphin. ###$p < 0.001$, significantly different from dorsomorphin for 1 day. $^{aaa}p < 0.001$. n = 6. Scale bar: 50 µm.

APPENDIX 2. STR PROFILES OF 661W CELL LINE.

To access the data, click or select the words "Appendix 2." The four curves correspond to STR loci labeled with four different fluorescent markers (blue=FAM, green=VIC, black=NED, red=PET). The abscissa (x-axis) represents the length of DNA fragments (unit: bp), reflecting the length of STR repeat sequences. The ordinate (y-axis) represents the intensity of fluorescent signals, indicating the amount of amplification products.

APPENDIX 3. COMPARE THE RESULT IN EXPASY DATABASE.

To access the data, click or select the words "Appendix 3." Name is the name of the cell line, used for intuitive identification of candidate cell lines. N° Markers is the number of STR loci detected, used to evaluate the comprehensiveness of the alignment. Score is the similarity score (percentage, with higher scores indicating higher STR typing matching), used for rapid screening of highly matching cell lines. STR 1–1, etc. are the alleles (repeat numbers) of each STR locus, used to verify genotype consistency locus by locus.

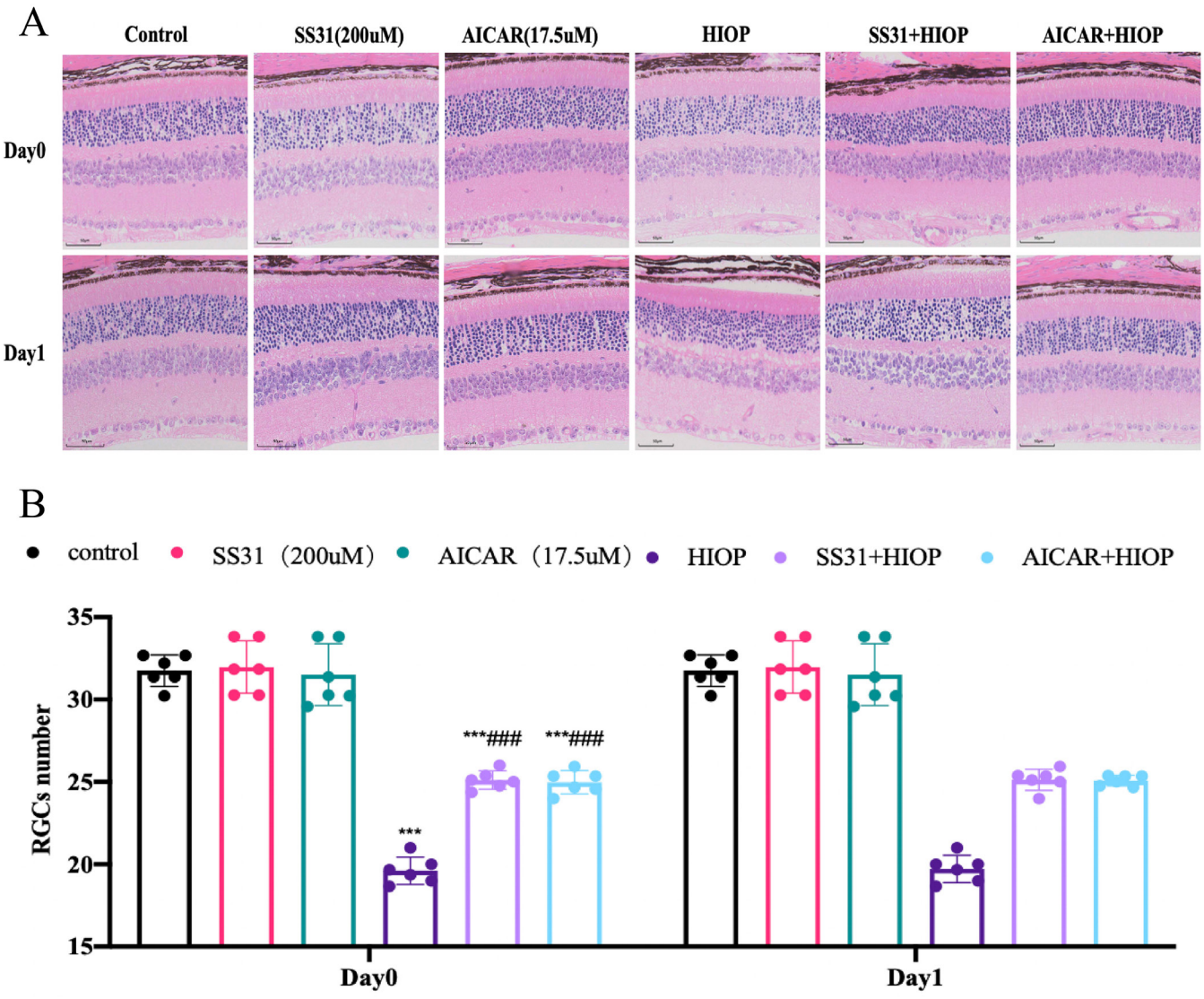

Figure 8. Intravitreous injection of SS31 and AICAR alleviated postperfusion retinal injury. Statistical analysis of retinal hematoxylin and eosin staining and retinal ganglion cell quantity in (**A**, **B**) SS31 (200 μM, 2 h) or AICAR (17.5 μM, 2 h) pretreated mice. *Significantly different from control. ***$p < 0.001$. #Significantly different from HIOP. ###$p < 0.001$. n = 6. Scale bar: 50 μm.

ACKNOWLEDGMENTS

Clinical Research Center for Ophthalmic Diseases of Shaanxi Province; Sanqin Talent Special Support Plan Innovation and Entrepreneurship team; Education Department of Shaanxi Provincial Government for Pathogenesis and Prevention Transformation Medicine for Glaucoma Innovation Team; Clinical Key Specialty of Shaanxi Province; Xi'an International Science and Technology Cooperation Base for Ophthalmology and Visual Science; Xi'an Key Laboratory for the Prevention and Treatment of Eye and Brain Neurologic Related Diseases; Ophthalmology Science and Technology Innovation Team of Xi'an Medical University; Key Disciplines of Xi'an Medical University. Availability of data and materials: The data sets used and/or analyzed during the current study are available from the corresponding author on reasonable request. Author contributions: YH designed and supervised the project; NC, R-XZ, QY, JJ, XW and YR performed research, analyzed the data; NC, R-XZ and YH interpreted the data and wrote the manuscript. All authors read and approved the final manuscript. Funding: This work was supported by National Natural Science Foundation of China (Grant No.82070964); Shaanxi Provincial Outstanding Youth Science Foundation Project (Grant No.2022JC-60); Youth Project of Natural Science Foundation of Shaanxi Province (Grant No.2025JC-YBQN-1225); Shaanxi Provincial Education Department Youth innovation team research project (Grant No. 24JP164). Xi 'an International science and technology cooperation base (Grant No.2024JH-GHJDZJ-0012); Open Research Funds of the State Key Laboratory of Ophthalmology (Grant No.83000–32030002); The Scientific Research and Innovation Capacity Enhancement Program of the Health Commission of Shaanxi Province (Grant No.2025YF-17). Commercial Relationships Disclosure: The authors declare that they have no competing interests. Ethics approval and consent to participate: Ethical approval was granted from the Research Ethics Committee of Xi'an Medical University, Shaanxi, China (Ethic Approval Number: XYLS2020110). All involving animal experiments and procedures were approved by the Ethical Committees for the use of laboratory animals at Xi'an Medical University, China.

REFERENCES

1. Weinreb RN, Aung T, Medeiros FA. The pathophysiology and treatment of glaucoma: a review. JAMA 2014; 311:1901-11. J[PMID: 24825645].

2. Kang JM, Tanna AP. Glaucoma. Med Clin North Am 2021; 105:493-510. J[PMID: 33926643].

3. Boland MV, Ervin AM, Friedman DS, Jampel HD, Hawkins BS, Vollenweider D, Chelladurai Y, Ward D, Suarez-Cuervo C, Robinson KA. Comparative effectiveness of treatments for open-angle glaucoma: a systematic review for the U.S. Preventive Services Task Force. Ann Intern Med 2013; 158:271-9. J[PMID: 23420235].

4. Zeng Z, You M, Fan C, Rong R, Li H, Xia X. Pathologically high intraocular pressure induces mitochondrial dysfunction through Drp1 and leads to retinal ganglion cell PANoptosis in glaucoma. Redox Biol 2023; 62:102687J[PMID: 36989574].

5. Pan L, Cho KS, Wei X, Xu F, Lennikov A, Hu G, Tang J, Guo S, Chen J, Kriukov E, Kyle R, Elzaridi F, Jiang S, Dromel PA, Young M, Baranov P, Do CW, Williams RW, Chen J, Lu L, Chen DF. IGFBPL1 is a master driver of microglia homeostasis and resolution of neuroinflammation in glaucoma and brain tauopathy. Cell Rep 2023; 42:112889J[PMID: 37527036].

6. Dammak A, Sanchez Naves J, Huete-Toral F, Carracedo G. New Biomarker Combination Related to Oxidative Stress and Inflammation in Primary Open-Angle Glaucoma. Life (Basel) 2023; 13:1455-J[PMID: 37511830].

7. Warren N, Mercer RN, Haddad J, Magrath G, Rocha KM. Corneal melt in conjunctival intraepithelial neoplasia. Am J Ophthalmol Case Rep 2020; 19:100689J[PMID: 32426552].

8. Ju WK, Perkins GA, Kim KY, Bastola T, Choi WY, Choi SH. Glaucomatous optic neuropathy: Mitochondrial dynamics, dysfunction and protection in retinal ganglion cells. Prog Retin Eye Res 2023; 95:101136J[PMID: 36400670].

9. Muench NA, Patel S, Maes ME, Donahue RJ, Ikeda A, Nickells RW. The Influence of Mitochondrial Dynamics and Function on Retinal Ganglion Cell Susceptibility in Optic Nerve Disease. Cells 2021; 10:1593-J[PMID: 34201955].

10. Zemirli N, Morel E, Molino D. Mitochondrial Dynamics in Basal and Stressful Conditions. Int J Mol Sci 2018; 19:564-J[PMID: 29438347].

11. Yapa NMB, Lisnyak V, Reljic B, Ryan MT. Mitochondrial dynamics in health and disease. FEBS Lett 2021; 595:1184-204. J[PMID: 33742459].

12. Jin JY, Wei XX, Zhi XL, Wang XH, Meng D. Drp1-dependent mitochondrial fission in cardiovascular disease. Acta Pharmacol Sin 2021; 42:655-64. J[PMID: 32913266].

13. Herzig S, Shaw RJ. AMPK: guardian of metabolism and mitochondrial homeostasis. Nat Rev Mol Cell Biol 2018; 19:121-35. J[PMID: 28974774].

14. Chen WR, Zhou YJ, Sha Y, Wu XP, Yang JQ, Liu F. Melatonin attenuates vascular calcification by inhibiting mitochondria fission via an AMPK/Drp1 signalling pathway. J Cell Mol Med 2020; 24:6043-54. J[PMID: 32368857].

15. Zhang X, Jia Y, Yuan Z, Wen Y, Zhang Y, Ren J, Ji P, Yao W, Hua Y, Wei Y. Sheng Mai San ameliorated heat stress-induced liver injury via regulating energy metabolism and AMPK/Drp1-dependent autophagy process. Phytomedicine 2022; 97:153920J[PMID: 35026620].

16. Liu J, Yan W, Zhao X, Jia Q, Wang J, Zhang H, Liu C, He K, Sun Z. Sirt3 attenuates post-infarction cardiac injury via inhibiting mitochondrial fission and normalization of AMPK-Drp1 pathways. Cell Signal 2019; 53:1-13. J[PMID: 30219671].

17. Hurley DJ, Irnaten M, O'Brien C. Metformin and Glaucoma-Review of Anti-Fibrotic Processes and Bioenergetics. Cells 2021; 10:2131-J[PMID: 34440899].

18. Birk AV, Liu S, Soong Y, Mills W, Singh P, Warren JD, Seshan SV, Pardee JD, Szeto HH. The mitochondrial-targeted compound SS-31 re-energizes ischemic mitochondria by interacting with cardiolipin. J Am Soc Nephrol 2013; 24:1250-61. J[PMID: 23813215].

19. Dai DF, Chen T, Szeto H, Nieves-Cintrón M, Kutyavin V, Santana LF, Rabinovitch PS. Mitochondrial targeted antioxidant Peptide ameliorates hypertensive cardiomyopathy. J Am Coll Cardiol 2011; 58:73-82. J[PMID: 21620606].

20. Szeto HH. Mitochondria-targeted cytoprotective peptides for ischemia-reperfusion injury. Antioxid Redox Signal 2008; 10:601-19. J[PMID: 17999629].

21. Zhao K, Zhao GM, Wu D, Soong Y, Birk AV, Schiller PW, Szeto HH. Cell-permeable peptide antioxidants targeted to inner mitochondrial membrane inhibit mitochondrial swelling, oxidative cell death, and reperfusion injury. J Biol Chem 2004; 279:34682-90. J[PMID: 15178689].

22. Zhang Z, Chen Z, Yang L, Zhang J, Li Y, Li C, Wang R, Wang X, Huang S, Hu Y, Shi J, Xiao W. Platelet Membrane-Encapsulated MSNs Loaded with SS31 Peptide Alleviate Myocardial Ischemia-Reperfusion Injury. J Funct Biomater 2022; 13:181-J[PMID: 36278650].

23. Yang Q, Xie W, Wang X, Luo J, Zhou Y, Cao H, Sun Q, Jiang L, Yang J. SS31 Ameliorates Podocyte Injury via Inhibiting OMA1-Mediated Hydrolysis of OPA1 in Diabetic Kidney Disease. Front Pharmacol 2022; 12:707006J[PMID: 36338294].

24. Reddy PH, Manczak M, Kandimalla R. Mitochondria-targeted small molecule SS31: a potential candidate for the treatment of Alzheimer's disease. Hum Mol Genet 2017; 26:1483-96. J[PMID: 28186562].

25. Yang L, Zhao K, Calingasan NY, Luo G, Szeto HH, Beal MF. Mitochondria targeted peptides protect against 1-methyl-4-phenyl-1,2,3,6-tetrahydropyridine neurotoxicity. Antioxid Redox Signal 2009; 11:2095-104. J[PMID: 19203217].

26. Yin X, Manczak M, Reddy PH. Mitochondria-targeted molecules MitoQ and SS31 reduce mutant huntingtin-induced mitochondrial toxicity and synaptic damage in Huntington's disease. Hum Mol Genet 2016; 25:1739-53. J[PMID: 26908605].

27. Wu X, Pang Y, Zhang Z, Li X, Wang C, Lei Y, Li A, Yu L, Ye J. Mitochondria-targeted antioxidant peptide SS-31 mediates neuroprotection in a rat experimental glaucoma model. Acta Biochim Biophys Sin (Shanghai) 2019; 51:411-21. J[PMID: 30811524].

28. Pang Y, Wang C, Yu L. Mitochondria-Targeted Antioxidant SS-31 is a Potential Novel Ophthalmic Medication for Neuroprotection in Glaucoma. Med Hypothesis Discov Innov Ophthalmol 2015; 4:120-6. J[PMID: 27350953].

29. Cai M, Li J, Lin S, Chen X, Huang J, Jiang X, Yang L, Luo Y. Mitochondria-Targeted Antioxidant Peptide SS31 Protects Cultured Human Lens Epithelial Cells against Oxidative Stress. Curr Eye Res 2015; 40:822-9. J[PMID: 25310141].

30. He Y, He B, Zhang R, Quan Z, Xu Y, Chen Z, Ren Y. The Mitochondrial-Targeted Peptide, SS31, Protects Murine 661W Cells from Oxidative Damage via Induction of Autophagy. J Biomed Nanotechnol 2020; 16:603-15. J[PMID: 32919481].

31. Zhou Y, Li M, Wang Z, Lin X, Xu Y, Feng S, Miao J. AMPK/Drp1 pathway mediates Streptococcus uberis-Induced mitochondrial dysfunction. Int Immunopharmacol 2022; 113:Pt A109413[PMID: 36461586].

32. Eisner V, Picard M, Hajnóczky G. Mitochondrial dynamics in adaptive and maladaptive cellular stress responses. Nat Cell Biol 2018; 20:755-65. J[PMID: 29950571].

33. Toyama EQ, Herzig S, Courchet J, Lewis TL Jr, Losón OC, Hellberg K, Young NP, Chen H, Polleux F, Chan DC, Shaw RJ. Metabolism. AMP-activated protein kinase mediates mitochondrial fission in response to energy stress. Science 2016; 351:275-81. J[PMID: 26816379].

34. Reddy PH, Manczak M, Yin X, Reddy AP. Synergistic Protective Effects of Mitochondrial Division Inhibitor 1 and Mitochondria-Targeted Small Peptide SS31 in Alzheimer's Disease. J Alzheimers Dis 2018; 62:1549-65. J[PMID: 29400667].

35. Wang X, Liu X, Ren Y, Liu Y, Han S, Zhao J, Gou X, He Y. PEDF protects human retinal pigment epithelial cells against oxidative stress via upregulation of UCP2 expression. Mol Med Rep 2019; 19:59-74. J[PMID: 30431098].

36. Mathew DJ, Livne-Bar I, Sivak JM. An inducible rodent glaucoma model that exhibits gradual sustained increase in intraocular pressure with distinct inner retina and optic nerve inflammation. Sci Rep 2021; 11:22880-J[PMID: 34819548].

37. Gross RL, Ji J, Chang P, Pennesi ME, Yang Z, Zhang J, Wu SM. A mouse model of elevated intraocular pressure: retina and optic nerve findings. Trans Am Ophthalmol Soc 2003; 101:163-9. , discussion 169–71.. J[PMID: 14971574].

38. Morrison JC, Cepurna WO, Johnson EC. Modeling glaucoma in rats by sclerosing aqueous outflow pathways to elevate intraocular pressure. Exp Eye Res 2015; 141:23-32. J[PMID: 26003399].

39. Laquis S, Chaudhary P, Sharma SC. The patterns of retinal ganglion cell death in hypertensive eyes. Brain Res 1998; 784:100-4. J[PMID: 9518569].

40. Moreno MC, Marcos HJ, Oscar Croxatto J, Sande PH, Campanelli J, Jaliffa CO, Benozzi J, Rosenstein RE. A new experimental model of glaucoma in rats through intracameral injections of hyaluronic acid. Exp Eye Res 2005; 81:71-80. J[PMID: 15978257].

41. Urcola JH, Hernández M, Vecino E. Three experimental glaucoma models in rats: comparison of the effects of intraocular pressure elevation on retinal ganglion cell size and death. Exp Eye Res 2006; 83:429-37. J[PMID: 16682027].

42. Ito YA, Belforte N, Cueva Vargas JL, Di Polo A. A Magnetic Microbead Occlusion Model to Induce Ocular Hypertension-Dependent Glaucoma in Mice. J Vis Exp 2016; 109e53731J[PMID: 27077732].

43. Morgan JE, Tribble JR. Microbead models in glaucoma. Exp Eye Res 2015; 141:9-14. J[PMID: 26116904].

44. Chen X, Rong Y, Jiang Y, Zhang Q, Xiang S, Chen Z, Chen W, Zhang H, Deng C, Wang J. Vitamin K1 Alleviates Retinal Inflammation Following Acute Ocular Hypertension by Modulating Microglial Ferroptosis. Invest Ophthalmol Vis Sci 2025; 66:46-[PMID: 40244608].

45. Zhang X, Li T, Zhang R, Li J, Wang K, Wu J. Downregulation of SARM1 Protects Retinal Ganglion Cell Axonal and Somal Degeneration Via JNK Activation in a Glaucomatous Model of Ocular Hypertension. Invest Ophthalmol Vis Sci 2024; 65:7-[PMID: 39499508].

46. Wu X, Yu N, Ye Z, Gu Y, Zhang C, Chen M, Wang K. Inhibition of cGAS-STING pathway alleviates neuroinflammation-induced retinal ganglion cell death after ischemia/reperfusion injury. Cell Death Dis 2023; 14:615-[PMID: 37726272].

47. Chen H, Deng Y, Gan X, Li Y, Huang W, Lu L, Wei L, Su L, Luo J, Zou B, Hong Y, Cao Y, Liu Y, Chi W. NLRP12 collaborates with NLRP3 and NLRC4 to promote pyroptosis inducing ganglion cell death of acute glaucoma. Mol Neurodegener 2020; 15:26-[PMID: 32295623].

Articles are provided courtesy of Emory University and The Abraham J. & Phyllis Katz Foundation. The print version of this article was created on 5 July 2026. This reflects all typographical corrections and errata to the article through that date. Details of any changes may be found in the online version of the article.